Under-expanded jets and dispersion in high pressure CO_2 releases from a large-scale pipeline

Xiaolu Guo [a], Xingqing Yan [a], Jianliang Yu [a†], Yongchun Zhang [b], Shaoyun Chen [b], Haroun Mahgerefteh [c], Sergey Martynov [c], Alexander Collard [c], Christophe Proust [d]

[a] School of Chemical Machinery and Safety,
Dalian University of Technology, Dalian, 116024, China

[b] School of Chemical Engineering,
Dalian University of Technology, Dalian, 116024, China

[c] Department of Chemical Engineering,
University College London, London WC1E 7JE, UK

[d] INERIS, Parc Technologique ALATA,
Verneuil-en-Halatte BP 2, 60550, France

[†]Corresponding Author
School of Chemical Machinery and Safety
Dalian University of Technology
No 2 Ling Gong Road
Dalian, 116024,China
e-mail: yujianliang@dlut.edu.cn
Tel.: +86 411 84986281
Fax: +86 13998576027

Manuscript submitted to *Energy*

September, 2016

Under-expanded jets and dispersion in high pressure CO_2 releases from a large-scale pipeline

Xiaolu Guo [a], Xingqing Yan [a], Jianliang Yu [a†], Yongchun Zhang [b], Shaoyun Chen [b], Haroun Mahgerefteh [c], Sergey Martynov [c], Alexander Collard [c], Christophe Proust [d]

Abstract

The widespread implementation of Carbon Capture and Storage (CCS) in industry will require extensive long-distance CO_2 pipeline networks to integrate the component technologies. The potential for pipeline rupture and leakage, possibly resulting in catastrophic accidents, will inevitably increase as networks become more extensive. The study of near-field source terms and dispersion behavior after pipeline rupture is an essential foundation of CO_2 pipeline risk assessment and will provide effective technical support for the implementation of large-scale CCS projects and contribute to pipeline safety. In the CO_2QUEST project under-expanded CO_2 jets, cloud dispersion characteristics and the formation of dry ice particles in the near field were investigated during releases from a 258 m long, fully instrumented pipeline. Experimental data including cloud temperature, CO_2 concentration and the visual evolution of the cloud (recorded on film), was gathered to investigate cloud behavior and to support future work in the field of CO_2 pipeline safety. Experiments included the release of gaseous and dense phase CO_2 through three orifice diameters: 15 mm, 50 mm and Full Bore Rupture (FBR). The lower limit of gaseous CO_2 concentration for adverse effects in humans is 5 % v/v. Safety distances from the release, based on this threshold concentration limit, are determined and reported for each experiment conducted.

Keyword: CO_2 release, Under-expanded jet, Dispersion, Large-scale pipeline.

1 Introduction

The importance of anthropogenic CO_2 in the atmosphere driving rapid global warming (https://www.iea.org/topics/climatechange/) and the recognition of the need to reduce CO_2 emissions are now widely accepted. This has motivated research into various emissions mitigation/reduction technologies, the most important of which is Carbon Capture and Storage (CCS) [1]. CCS has the greatest potential to reduce atmospheric emissions of CO_2, mitigating some negative effects of the continued use of fossil fuels until clean energy technologies can be implemented [2]. Its rapid deployment has the potential to contribute significantly to limiting the rise in global temperatures to 2 °C above pre-industrial levels [3]. Pipeline transportation of CO_2 for CCS is accepted as the safest and most efficient transportation option [4]. However CO_2 pipelines present a significantly different risk profile compared to, for example, hydrocarbon pipelines. Notably CO_2 is denser than air, odorless, colorless and not flammable. The acute health effects of CO_2 are dependent on the concentration in the air and duration of exposure, concentrations of 10 % v/v will render an adult unconscious after 1 minute and exposure to concentrations of 20 % v/v or greater is instantaneously fatal [5,6,7]. A threshold value of 5 % v/v concentration is assumed to be the lower limit for adverse human effects [27]. Safety distances in published risk assessments for underground high pressure CO_2 pipelines vary from less than 1 m to 7.2 km as a result [8]. This large variation in the safety distance has significant implications for pipeline design, routing, operation, maintenance and security.

In the event of a rupture in a high pressure CO_2 pipeline a significant mass of inventory may

be discharged very rapidly, possibly before the leak is detected. Due to its relatively high Joule Thomson expansion coefficient, CO_2 may reach temperatures as low as -70 °C during a pipeline release. This has the potential to induce brittle fracture in a pipe wall in addition to the initial risk of ductile fracture [9], as well as introducing the possibility of dry ice formation in the pipeline and near-field dispersion zone [10]. During a prolonged release a fully expanded dispersion cloud will be connected to the pipeline rupture by a highly under-expanded jet containing a Mach disk orthogonal to the flow direction [11]. External to the pipeline, solid CO_2 particles are most likely to form in the jet. If solid CO_2 is formed it will subsequently sublime and mix with the vapor cloud. Transient cloud properties may be significantly affected by the formation or absence of solid CO_2 in the under-expanded jet. In the process of mixing with the atmosphere the momentum of the jet diminishes and dispersion will continue as a vapor cloud dispersion [12].

Many experimental studies have been conducted to establish a clear understanding of the hazards associated with the failure of CO_2 pipelines. As part of the CO_2PipeHaz project, INERIS [13-15] built a 2 m^3 spherical vessel connected to a 9 m long pipe with an inner diameter of 50 mm. This apparatus was used to measure temperatures and gas concentrations in the dispersion region during outflow from the pipe in order to guide large scale experimental CO_2 release studies. An important observation from this work was that significant solids are generated within the near-field of dense phase releases, despite the release itself containing no dry ice. Witlox et al. [23,24] presented experimental work conducted by BP and Shell during the CO_2 PIPETRANS JIP, including both high-pressure

steady-state and time-varying cold CO_2 releases and high-pressure time-varying supercritical hot CO_2 releases. For all cases solid CO_2 formed in the dispersion area and was observed to sublime rapidly and no rainout was predicted. Xie et al. [16,17] developed a 23 m long circulating pipeline with a 30 mm inner diameter to study the pipeline leakage process of supercritical CO_2 in a vertical direction. A typical highly under-expanded jet flow structure was observed. However, this structure disappeared as the orifice size increased. DNV-GL [18] investigated the discharge of liquid CO_2 from a 0.5 m^3 pressurized vessel equipped with an actuator valve. The results showed that the CO_2 concentrations near the orifice depend mainly on the jet shape rather than the mass flow rate. The concentrations at 9 and 15 m from the release point tended to increase continuously while saturated liquid was being discharged, and then to drop with the transition to vapor outflow. Xing et al [19] used a series of scaling rules based on field experiments of CO_2 dispersion to simulate large scale CO_2 blowouts. Through comparison with the k–ϵ model and statistical performance indicators, it was concluded that the scaling rules appeared applicable to field experiments of accidental release.

Several experimental research programs have been performed at the Spadeadam Test Site in Cumbria, UK. The COSHER JIP [20] performed a large scale pipeline rupture test using a 226.6 m long pipeline loop built with 219.1 mm diameter steel pipe and fed from both ends by a 148 m^3 reservoir of CO_2. The results showed that a visible cloud reached a maximum height of about 60 m and a maximum distance from the rupture location of about 400 m. Pseudo-steady CO_2 concentrations were reached at up- and downwind locations in the

near-field in low wind speed conditions, but not in the far-field. Wareing et al. [21,22] studied the venting of dense and gas phase CO_2 through a single, straight vertical vent pipe within the framework of the COOLTRANS research program. The experimental data used in these releases was used to develop a CO_2 dispersion model.

As part of the CO_2QUEST project [25,26], this paper reports work to study highly under-expanded jets and the dispersion characteristics of gaseous and dense phase CO_2 during sudden release from a pipeline. Six large-scale CO_2 release experiments are reported. The pipeline used was 258 m long with an inner diameter of 233 mm, three orifice sizes were used in experiments (15 mm, 50 mm and Full Bore Rupture). The experimental studies provide a detailed understanding of the hazards presented by CO_2 releases, the data recorded could be used to validate outflow and dispersion models.

2 Experiments

2.1 Experimental setup

Figure 1 shows a schematic representation of the CO_2 pipeline employed for conducting the release experiments. The pipeline was 257 m long with and inner diameter of 233 mm and a wall thickness of 20 mm. It was built with 16MnR low temperature carbon steel and had a maximum pressure rating of 16 MPa. Concrete foundations and supports rigidly clamped the pipeline 1.3 m above the ground. Additionally, a reinforcing anchor device capable of resisting an acting force of 400 kN was designed to prevent movement of the pipeline during experiments. The pipeline was wrapped in 50 kW heating tape and a 50 mm thick layer of thermal insulation. The heating system could warm the inventory to a maximum temperature

of 40 °C.

A 1 m long dual-disc blasting pipe built using grade 304 stainless steel was attached to one end of the pipeline and used to initiate experiments. The blasting device consisted of two rupture discs and two disc holders, a solenoid valve, two pipe sections and an end flange. Replaceable flanges with different sizes of pre-prepared (circular) orifices were installed in the blasting pipe for experiments, orifice diameters of 15 mm, 50 mm and Full Bore Rupture (FBR) were used. Each orifice was cut in the center of the flange. To initiate release experiments disk A was ruptured by reducing the pressure in section 1 of the blasting pipe (see Figure 1). This increased the pressure differential across disk B causing it to rupture, the net result is the essentially instantaneous opening of the pipeline.

The pipeline was charged and experiments conducted as follows:

(1) Purge the pipeline using gaseous CO_2.

(2) Charge the pipeline with the previously calculated mass of CO_2 required for the experiment.

(3) Once charged, use the heating system to alter inventory conditions to those desired for the experiment.

(4) Isolate the experimental field.

(5) Initiate the experiment using the dual-disc blasting device and record the desired experimental data.

(6) After the release is complete and instruments indicate the cloud is fully dispersed prepare the experimental field for the next release.

2.2 Pipeline instrumentation

An overhead schematic view of the locations and types of instruments in the dispersion zone is shown in Figure 2. Thermocouples and CO_2 concentration sensors were both arranged on vertical tubes at the same height as the pipeline, as shown in Figure 3. T-type thermocouples with an uncertainty of ±1 °C, a measurement range of -200 °Cto 400 °C and response times of 100 ms were used. The CO_2 concentration sensors used were COZIR-W type manufactured by Gas Sensing Solutions Ltd (GSS). Their measurement range was 0–100 %, their accuracy was ±3 % and their response time was 4 s.

Two data acquisition systems ran simultaneously during experiments, an NI cRIO-9025 system which was used to sample the thermocouples while an RS485 communication system was used to sample the CO_2 concentration sensors. The NI cRIO-9025 system consisted of one 9025 and one 9144 chassis and two NI 9213 thermocouple input modules. The RS485 communication bus adopted a twist-pair with RVVSP 2×2×0.5 mm^2 and a master-slave half duplex mode. The data-acquisition code was programmed using LabVIEW software from National Instruments UK.

A weather station was established to record ambient temperature, pressure, humidity, wind speed and direction. The ambient pressure was measured using a QA-1 air pressure sensor with an accuracy of ±0.03 kPa and a range of 55 kPa to 106 kPa. The ambient temperature and humidity were measured using PTS-S environment monitoring sensors, each with an uncertainty of ±0.1 °C and ±0.2 % and a range of -50 °C to 80 °C and 0 to 100 % respectively.

The wind speed and direction were measured using an EC-A1 ultrasonic wind sensor with an accuracy of ±0.01 m/s and ±1° and a range of 0 to 60 m/s and 0 to 360°. Several digital HD video cameras and a Phantom 2 Vision aerial drone were used to record the evolution of the visible cloud during experiments.

2.3 Experiments conducted

Six CO_2 release experiments were performed to investigate dispersion behaviour during the release of gaseous and dense phase CO_2 from a pipeline. Orifice diameters of 15 mm, 50 mm and Full Bore Rupture were used. The purity of the CO_2 was 99.9%. The initial and environmental conditions of six tests are presented in Table 1. For tests 1 and 4 the ambient pressure, temperature, wind speed and direction fluctuated violently as result of unstable atmospheric conditions during the long depressurization. Other tests were carried out in more stable ambient conditions.

3 Experimental results

3.1 Gas phase tests

3.1.1 Visible cloud development

Based on the experimental data, the development of the visible cloud may be divided into three stages: (I) rapid expansion, (II) the metastable stage and (III) the slow attenuation stage. For tests 1, 2 and 3 the duration times for the respective clouds in each stage of development are shown in Table 2 together with the total depressurization times.

Figures 4, 5 and 6 show the development of the visible cloud for tests 1, 2 and 3 respectively. As may be observed in each figure the released gas may be seen as a white cloud with a base

touching the rupture plane. Although the inventory is colourless, the significant cooling of the CO_2 as it expanded passing through the orifice and in the under-expanded jet resulted in the formation of solid CO_2 particles. These particles remained entrained in the cloud and did not rain out. For tests 1 and 2, the visible cloud was fully developed during the rapid expansion phase and its dimensions remained relatively stable during the metastable stage. During the attenuation stage the expansion angle of the jet and overall dimensions of the cloud decreased. The white visible cloud disappeared in the forefront of the jet flow, indicating that the dry ice partcles had gradually sublimated during diffusion.

For test 2 the jet travelled in a straight line along the axial direction throughout the experiment, the divergent angle remained circa 11^o throughout. In the metastable stage the visible cloud dimensions remained relatively constant with a length of circa 10 m and a maximum radius of circa 1.5 m. As may be observed at 45 s and 60 s (figure 5), the intercepting shock and the Mach disc were clearly visible in the jet flow.

For test 3 jet velocities are indicated in figure 6 for the first 0.8 s. In the rapid expansion stage the visible white cloud rapidly expanded, entraining dry ice particles and condensed water vapour. The expanding jet velocity simultaneously decreased as the distance from the rupture increased. The visible cloud reached a maximum length of circa 40 m. The divergent angle of the jet was circa 18^o. In the slow attenuation stage the visible white cloud and the mixture of gaseous CO_2, air and raised dust separated. Even when no white cloud was visible, a measurable CO_2 cloud continued to spread, relying on momentum, wind and body forces to

do so. As test 3 involved an FBR the dry ice particles formed were spread farther, allowing the considerable diffusion velocity and range of this test to be observed.

3.1.2 Temperature distribution

Figure 7 shows the temperature evolution along the axial line of the discharge area in tests 1, 2 and 3. In all cases, after rupture the ambient temperature in the far-field dropped as a result of the expansion of the escaping gas and the sublimation of dry ice particles. The cloud temperature along the axis of the release gradually rose as the distance from the orifice increased due to the reduction of the cloud velocity and the fraction of dry ice further from the orifice. When the release was complete the temperature of the CO_2 gradually increased to ambient as it continued to mix with air. For test 1, the temperature distribution in the dispersion region was small but it fluctuated as the smaller jet in this experiment was more significantly affected by the unstable atmospheric environment. For test 2, the temperature contour lines quickly extended along the axial direction and reached the maximum values at 15 s after rupture. For test 3 the rates of extension and retreat of the temperature contour lines were similar as a result of the violent mixing of the escaping gas and air and the extremely unstable atmosphere in the full bore release. The maximum temperature drops observed 4 m from the orifice were 4.2 °C, 5.5 °C and 17.6 °C, occuring at the times of 35 s, 15 s and 7 s for tests 1, 2 and 3 respectively. The lowest cloud temperatures were only observed for short times, while the maximum temperature drop ampitudes became bigger with increasing orifice diameter due to the more violent mixing of the escaping gas and air.

Figure 8 shows the lowest temperature distribution in the discharge area for tests 1, 2 and 3. The y direction is along the jet axis and the x direction is horizontal distance. Obviously, the temperature of the escaping gas increased along the x and y directions in the discharge area. The lengths of the temperature contour lines along the x direction were much longer than those along the y direction while the temperature gradients along the x direction were much lower. For the 23 °C and 24 °C contours recorded for test 1, the 23 °C , 24 °C and 25 °C contours recorded for test 2, and the 10 °C , 13 °C and 16 °C contours recorded for test 3, the length ratios between the y and x directions were 16.1, 12.9, 33.5, 29.6, 21.3, 58.3, 30.4 and 24.1 for each contour line respectively. This confirms that the temperature contour lines along the y direction were much larger than that along the x direction as a result of the much greater axial velocity of CO_2 compared to radial velocity. The length ratio between the temperature contour lines along the x and y directions became larger with increasing orifice diameter. This was mainly because the jet velocities and distribution range became greater with the increase in orifice diameter. For tests 1, 2 and 3, the length and width of the low-temperature zones were predicted to be 13 by 2.5 m, 16 by 2.2 m, and 20 by 2.5 m respectively.

3.1.3 CO_2 concentration dispersion

Figure 9 shows the evolution of concentration along the axial direction in tests 1, 2 and 3. As may be observed, the contours of CO_2 concentration remained at their maximum extent through the metastable state. The closer the distance to the orifice, the longer the exposure to 5 % v/v concentrations of CO_2. The start time of the contour of low CO_2 concentration was

earlier than that of high CO_2 concentration, this was due to the response lag of the CO_2 concentration sensors to the high-velocity gas. The response lag had little influence on the assessment of dangerous concentration distances.

For test 1, the 5 % CO_2 concentration contour reached a maximum distance of 9.2 m from the release orifice, thus the safety distance along the axial direction should be less than 10 m in test 1. For test 2, at the end of the release (159 s), CO_2 concentrations within the measurement area stayed above 3 % concentration, decreasing below 1 % concentration by 207 s after the rupture. Thus for test 2 the safety distance along the axial direction should be at least 12 m. For test 3, the 5 % CO_2 concentration contour quickly reached its maximum extent at 13 s. CO_2 concentrations at a distance of 5 m from the release orifice reached 30.1 % at the end of the release (15 s) and reached a maximum value at 27 s. At this distance the CO_2 concentration remained above 5 % v/v until 150 s after rupture. This persistent concentration was caused by the sublimation of the dry ice particles in the discharge area. The safety distance in test 3 should be at least 25 m. It was obvious that the larger discharge diameter brought a greater amount of discharged CO_2 into the dispersion region over a given time interval.

3.2 Dense phase tests

3.2.1 Visible cloud development

For tests 4, 5 and 6 the duration times for the respective clouds in each stage of development are shown in Table 3 together with the total depressurization times. Compared with the gas

phase tests, the duration times of the clouds in each stage of evolution were longer, as expected.

Figures 10, 11 and 12 show the development of the visible clouds for tests 4, 5 and 6 respectively. The recorded dimensions of the test 4 dispersion cloud at various times are given in table 4. The data reports a gradual increase in the length and height of the visible cloud as the expanding velocity decreased from an initial peak. For tests 5 and 6 cloud dimensions are also reported in table 4. The data indicates that the size and expanding velocity of the visible cloud increased as the orifice size increased. For test 4, the dimensions of the visible cloud reached their maximum at 9 s. For tests 5 and 6, the clouds reached their maximum horizontal dimensions at 6 s and 5 s respectively, although maximum visible cloud heights were achieved earlier (see table 4). The dispersion clouds therfore continued to expand horizontally after reaching their maximum visible height, solid CO_2 formation and gas density contributed to this behaviour. Orifice size had a clear influence on visible cloud height; the angle of reflection of the jet from the ground was greater as the orifice size increased, resulting in higher dispersion clouds.

For the dense phase tests 4, 5 and 6, the divergent angles of the jets were greatest at the moment of rupture and decreased gradually during blowdown. In the rapid expansion stage the axial length of the jet increased quickly and the leading edge of the jet expanded along an arc frontage. In the metastable stage the dimensions of the cloud remained essentially stable and the forward edge of the cloud adopted a fan-shape. The heavy gas effect started prompting the free diffusion of CO_2 in low-lying areas. In the slow attenuation stage, as the

expanding jet velocity decreased cloud diffusion increasingly depended on residual momentum. The size of the visible cloud began to decay and the attenuation velocity decreased. Compared to the gas phase tests the visible cloud produced in the dense phase tests had a much wider dispersion range and a greater amount of dry ice particles and condensed water vapour were formed. The amount of condensed water vapour entrained in the jet was dependent on the ambient humidity and the degree of cooling of the CO_2 in the jet (and therefore on the initial inventory pressure).

3.2.2 Temperature distribution

Figure 13 shows the temperature evolution along the axial line of the discharge area in tests 5 and 6. For test 4 the temperatures in the dispersion area were not recorded due to instrument failure. For test 5, the temperature contour lines quickly extended along the axial direction and reached their maximum extent at 13 s. The temperature drop amplitude 5 m from the rupture reached 31 °C, a larger drop than in test 2. For test 6, the temperature drop amplitude reached 24 °C at 3 s, a larger drop than that at the same time for test 3, and reached a maximum value of 102 °C at 17 s. This time was later than the equivalent time in test 3 (3 s) due to the continuous sublimation of dry ice particles in test 6. The results indicate similar behaviour in the temperature evolution along the release direction between the dense and gas phase tests. However, it is clear that for a given orifice size the low-temperature areas in the dense phase tests covered a greater area than in the gas phase tests.

Figure 14 shows the distribution of low temperature zones in the discharge area for tests 5 and 6. The y direction is along the jet axis and x direction is the horizontal distance. The

overall trend was for the temperature gradient along the x direction to be much more abrupt than along the y direction, while the lengths of the temperature contour lines along the x direction were much longer than those along the y direction. For 0 °C, 3 °C, 6 °C and 9 °C in test 5, the length ratios between the temperature contour lines along the y direction and the x direction were close to 10.1. This indicated that the temperature distribution shifted to the right due to the effect of the southeast wind. For the -40 °C, -30 °C, -20 °C and -10 °C contour lines in test 6, the length ratios between the y and x directions were 96.6, 45.6, 32.7 and 27.1 respectively. This shows that the diffusion velocity in the FBR release with dense phase CO_2 was extremely fast, as a result the temperature distribution in the resulting dispersion cloud could be considered essentially axisymmetric. According to the contour extending trend in tests 5 and 6, it was predicted that the maximum length and width of the low-temperature zone was 16 m by 3 m and 30 m by 5 m in tests 5 and 6 respectively.

3.2.3 CO_2 concentration dispersion

Figure 15 shows the evolution of CO_2 concentration along the axis of release in tests 4, 5 and 6. For test 4, CO_2 concentration 5 m from the release orifice reached 5 % v/v 15 s after rupture and remained at this quasi steady state level until 3200 s. The greatest extent of the 5 % concentration contour was 19.2 m from the orifice, reached 263 s after rupture. Therefore the safety distance along the release direction should be circa 20 m for test 4. For test 5, the concentration contour lines fluctuated intermittently due to the varying southeast wind. The 5 % v/v concentration contour extended 12 m from the release orifice by 6 s and remained above 5 % at this distance until the end of the release (482 s). The safety distance along the

release direction in test 5 should be circa 60 m. For test 6, CO_2 concentration contours began to extend from the rupture after 6 s and reached their farthest point at 15 s. At the end of the release (40 s) CO_2 concentrations at a distance of 60 m from the release orifice had remained above 5 % v/v concentration as a result of the continual sublimation of the dry ice particles. 61 % v/v concentration was achieved 20 m from the orifice (the maximum at this location) earlier than a 100 % v/v concentration was achieved 5 m from the orifice. This suggested that due to dry ice sublimation and the response time of the sensors, the duration of exposure to maximum CO_2 concentrations was longer as the distance to the orifice decreased. The safety distance along the release direction in test 6 reached circa 160 m.

4 Discussion

This paper studied highly under-expanded jets and their dispersion characteristics during the release of gaseous and dense phase CO_2 from a large-scale pipeline. Such a large capacity pipeline was essential as it permitted long duration experiments to be performed and large amounts of data to be captured for analysis. A great many sensors were used to monitor the formation of the visible cloud and the variation of temperatures and concentrations in the far-field. The research results of near-field source terms and dispersion behavior in this study are necessary and of paramount importance for assessing safety distances and the impact of CO_2 pipeline releases on the surrounding environment.

Rupture or puncture of a high pressure CO_2 pipeline will almost certainly result in a high-velocity jet from the pipeline and the transition of the inventory through different physical states. For high pressure pipelines, sonic velocity will likely be reached at the outlet

of the pipe and the resulting free jet will therefore be sonic. This would lead to a highly under expanded flow that contains a Mach disk, the precise form of which depends on the ratio of the exit to atmospheric pressure. For CO_2 releases, the temperature and pressure decrease that accompanies inventory expansion will lead to the formation of dry ice particles and condensed water vapor. Likewise, sublimation of dry ice particles will result in heat removal from the gas phase and an associated temperature decrease. Formation of solid CO_2 will affect the shape and properties of a CO_2 cloud in ways different to a gas/liquid cloud [28]. In addition, ground topography and physical objects, as well as wind direction, may have a significant influence on the spread and movement of a CO_2 cloud. These extremely complicated phenomena may be expected during the dispersion process of gaseous or dense phase CO_2 during sudden release. High pressure CO_2 dispersion modelling therefore requires appropriate source terms, accurate turbulence modeling, a three-phase accurate equation of state, to account for heat transfer between the ground and the flowing fluid and precise particle tracking techniques for estimating the amount of solid CO_2 [29-31]. No mathematical model is currently capable of predicting all these phenomena during complex releases.

Currently, the authors focus on experimental research over theoretical analysis. This and related large-scale experimental work contributes basic data to CO_2 dispersion research and can be used to validate outflow, near-field and far field dispersion models. Experimental characterisation of the temperatures in the immediate vicinity of a release will also be performed to enable estimation of the risk to piping, plant or structures from low temperature embrittlement. For the design, construction and operation of new high pressure CO_2 pipelines

through populated areas, the safety distance to the release point, measured along the release axis, should be consistent with the 5 % v/v concentration threshold in the dispersion cloud. This distance is critically important when performing consequence failure analysis and quantifying major hazards for CO_2 pipelines. More sophisticated experimental and theoretical studies will be conducted on dispersion behavior during sudden releases in the future.

5 Conclusions

This article has presented the results of a large-scale experimental study of under-expanded jets and dispersion characteristics of gaseous and dense phase CO_2 following pipeline rupture through three orifice sizes (15 mm, 50 mm and Full Bore Rupture). The following conclusions were drawn from the study:

(1) A highly under-expanded flow containing a Mach disk was developed during the release of high pressure CO_2. A large quantity of dry ice particles formed in the near-field due to Joule-Thomson cooling, these were carried into the far-field. The dispersing cloud was made visible by both these dry ice particles and condensing water vapor. The dry ice sublimed rapidly and did not settle.

(2) After rupture, the ambient temperature in the far-field dropped as a result of the expansion of the escaping gas and the sublimation of the dry ice particles. The cloud temperature along the release axis gradually rose as the expanding velocity and the fraction of dry ice decreased along this axis. For given initial conditions, as the orifice diameter increased the degree of cooling and the dispersion distance of CO_2 in the discharge area, and therefore the safety distance, increased.

(3) Compared to the gas phase tests, the visible cloud produced in dense phase tests entrained more condensed water vapour, included a greater mass of dry ice and had a much wider dispersion range. The footprint of the low-temperature areas of the cloud and the safety distances in the dense phase tests were also much greater than that in the gas phase tests. The dense CO_2 gas was observed to gather in low lying areas after release when not dispersed by the wind.

Acknowledgement

The authors would like to acknowledge the funding received from the European Union Seventh Framework Programmes FP7-ENERGY-2009-1 under grant agreement number 241346 and FP7-ENERGY-2012-1STAGE under Grant agreement 309102.

References

[1] Haszeldine RS. Carbon capture and storage: how green can black be? Nature 2009; 325:1647-1652.

[2] Munkejord ST, Hammer M, Løvseth SW. Intergovernmental panel on climate change, carbon capture & storage, ISBN 92-9169-119-4. Appl Energy 2016; 169:499–523.

[3] IEA, Energy Technology Perspectives 2008, Paris: France, 2008.

[4] Chong FK, Lawrence KK, Lim PP, Poon MCY, Foo DCY, Lam HL, Tan RR PP. Planning of carbon capture storage deployment using process graph approach. Energy

2014; 76:641-651.

[5] Iribarren D, Petrakopoulou F, Dufour J. Environmental and thermodynamic evaluation of CO2 capture, transport and storage with and without enhanced resource recovery. Energy 2013; 50:477-85.

[6] Duncan IJ, Wang H. Estimating the likelihood of pipeline failure in CO_2 transmission pipelines: New insights on risks of carbon capture and storage. Int J Greenh Gas Con 2014; 21: 49-60.

[7] Brown S, Beck J, Mahgerefteh H. Global sensitivity analysis of the impact of impurities on CO_2 pipeline failure. Reliab Eng Syst Safe. 2013; 115: 43–54.

[8] Molag M, Dam C. Modelling of accidental releases from a high pressure CO_2 pipelines. Energy Procedia 2011; 4:2301-2307.

[9] Botros KK, Hippert E Jr, Craidy P. Measuring decompression wave speed in CO_2 mixtures by a shock tube. Pipelines International 2013; 16:22-28.

[10] Mazzoldi A, Hill T, Colls JJ. CO_2 transportation for carbon capture and storage: Sublimation of carbon dioxide from a dry ice bank. Int J Greenh Gas Con 2008 2:210-218.

[11] Witlox HWM, Harper M, Oke A. Modelling of discharge and atmospheric dispersion for carbon dioxide releases. J Loss Prevent Proc 2009; 22:795-802.

[12] Witkowski A, Rusin A, Majkut M, Rulik S, Stolecka K. Comprehensive analysis of pipeline transportation systems for CO_2 sequestration. Energ Convers Manage 2013; 76: 665-673.

[13] Woolley RM, Fairweather M, Wareing CJ, Falle SAEG, Proust C, Hebrard J, Jamios D. Experimental measurement and Reynolds-averaged Navier–Stokes modelling of the near-field structure of multi-phase CO_2 jet releases. Int J Greenh Gas Con 2013; 18:139–149.

[14] Gant SE, Narasimhamurthy VD, Skjold T, Jamois D, Proust C. Evaluation of multi-phase atmospheric dispersion models for application to Carbon Capture and Storage. J Loss Prevent Proc 2014; 32:286-298.

[15] Woolley RM, Fairweather M, Wareing CJ, Falle SAEG, Mahgerefteh H, Martynov S, Brown S, Narasimhamurthy VD, Storvik IE, Sælen L, Skjold T, Economou IG, Tsangaris DM, Boulougouris GC, Diamantonis NI, Cusco L, Wardman M, Gant SE, Wilday J, Zhang YC, Chen SY, Proust C, Hebrard J and Jamois D. CO_2PipeHaz: quantitative hazard assessment for next generation CO_2 pipelines. Energy Procedia 2014, 63:2510–2529.

[16] Xie QY, Tu R, Jiang X, Li K, Zhou XJ. The leakage behavior of supercritical CO_2 flow in an experimental pipeline system. Appl Energy 2014; 130:574-580.

[17] Li K, Zhou XJ, Tu R, Xie QY, Jiang X. The flow and heat transfer characteristics of supercritical CO_2 leakage from a pipeline. Energy 2014; 71:665-672.

[18] Ahmad M, Osch MB, Buit L, Florisson O, Hulsbosch-Dam C, Spruijt M, Dacolio F. Study of the thermohydraulics of CO_2 discharge from a high pressure reservoir. Int J Greenh Gas Con 2013; 19:63-73.

[19] Xing J, Liu ZY, Huang P, Feng CG, Zhou Y, Sun RY, Wang SG. CFD validation of

scaling rules for reduced-scale field releases of carbon dioxide. Appl Energy 2014; 115: 525-530.

[20] Ahmad M, Lowesmith B, Koeijer Gd, Nilsen S, Tonda H, Spinelli C, Cooper R, Clausen S, Mendes R, Florisson O. COSHER joint industry project: Large scale pipeline rupture tests to study CO_2 release and dispersion. Int J Greenh Gas Con 2015; 37:340–353.

[21] Wareing CJ, Fairweather M, Falle SAEG, Woolley RM. Validation of a model of gas and dense phase CO_2 jet releases for carbon capture and storage application. Int J Greenh Gas Con 2014; 20:254-271.

[22] Wen J, Heidari A, Xu BP, Jie HG. Dispersion of carbon dioxide from vertical vent and horizontal releases—A numerical study. J Process Mechanical Engineering 2013; 227:125-139.

[23] Witlox HWM, Harper M, Oke A, Stene J. Validation of discharge and atmospheric dispersion for unpressurised and pressurised carbon dioxide releases. Process Saf Environ 2014; 92:3-16.

[24] Witlox HWM, Harper M, Oke A, Stene J. Phast validation of discharge and atmospheric dispersion for pressurised carbon dioxide releases. J Loss Prevent Proc 2014; 30:243-255.

[25] Brown S, Martynov S, Mahgerefteh H, Fairweather M, Woolley RM, Wareing CJ, Falle SAEG, Rutters H, Niemi A, Zhang YC, Chen SY, Besnebat J, Shah N, Dowell NM, Proust C, Farret R, Economou IG, Tsangaris DT, Boulougouris GC, Wittenberghe JV. CO_2QUEST: Techno-economic assessment of CO_2 quality effect on its storage and

transport. Energy Procedia 2014; 63:2622-2629.

[26] Guo XL, Yan XQ, Yu JL, Zhang YC, Chen SY, Mahgerefteh H, Martynov S, Collard A, Proust C. Pressure response and phase transition in supercritical CO2 releases from a large-scale pipeline. Appl Energy 2016; 178:189-197.

[27] Kruse H, Tekiela M. Calculating the consequences of a CO_2-pipeline rupture. Energy Convers 1996; 37:1013-1018.

[28] Harper P, Wilday J, Bilio M. Assessment of the Major Hazard Potential of Carbon Dioxide (CO_2). Health and Safety Executive 2011; 1-28.

[29] Zhou XJ, Li K, Tu R, Yi JX, Xie QY, Jiang X. A modelling study of the multiphase leakage flow from pressurized CO_2 pipeline. J Hazard Mater 2016; 306:286-294.

[30] Wareing CJ, Woolley RM, Fairweather M, Falle SAEG. A composite equation of state for the modeling of soniccarbon dioxide jets in carbon capture and storage scenarios. AIChE J 2013; 59:3928-3942.

[31] Wareing CJ, Fairweather M, Falle SAEG, Woolley RM. Modelling punctures of buried high-pressure dense phase CO_2 pipelines in CCS applications. Int J Greenh Gas Con 2014; 29:231-247.

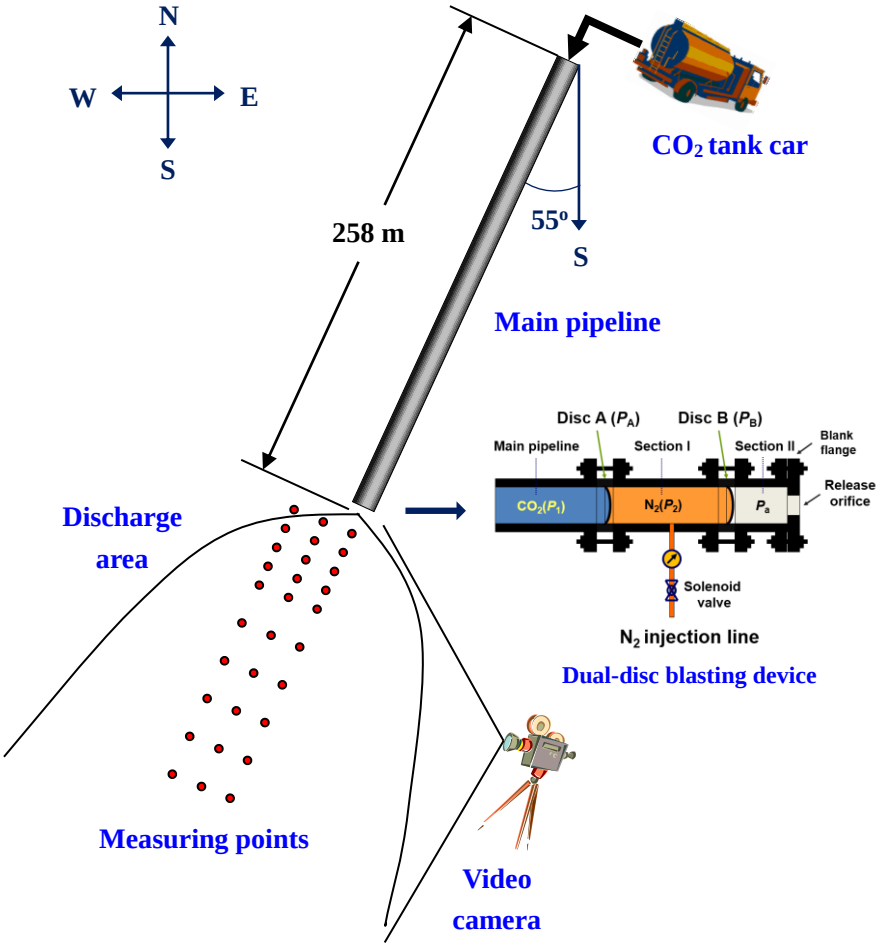

Fig. 1 Process flow.

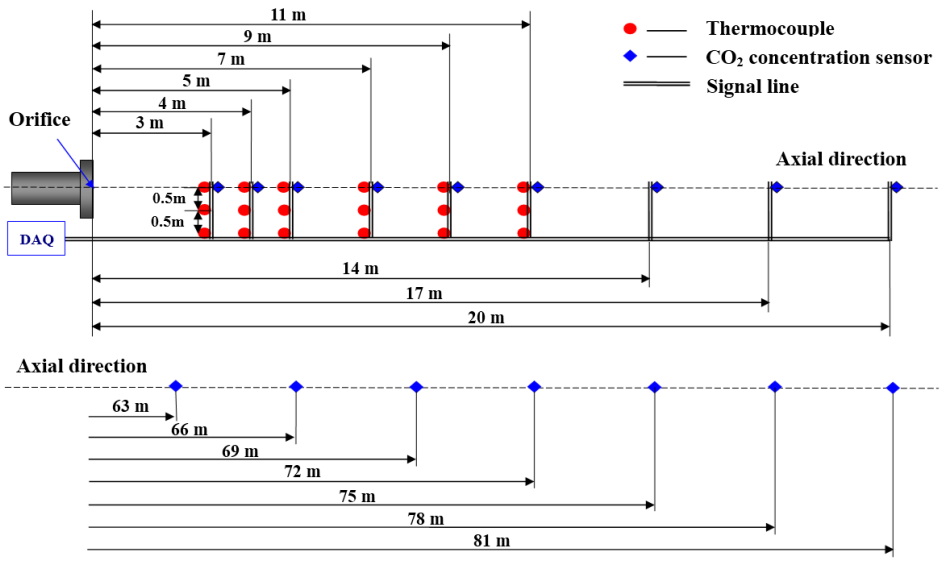

Fig. 2 Distribution of measurement points in discharge area.

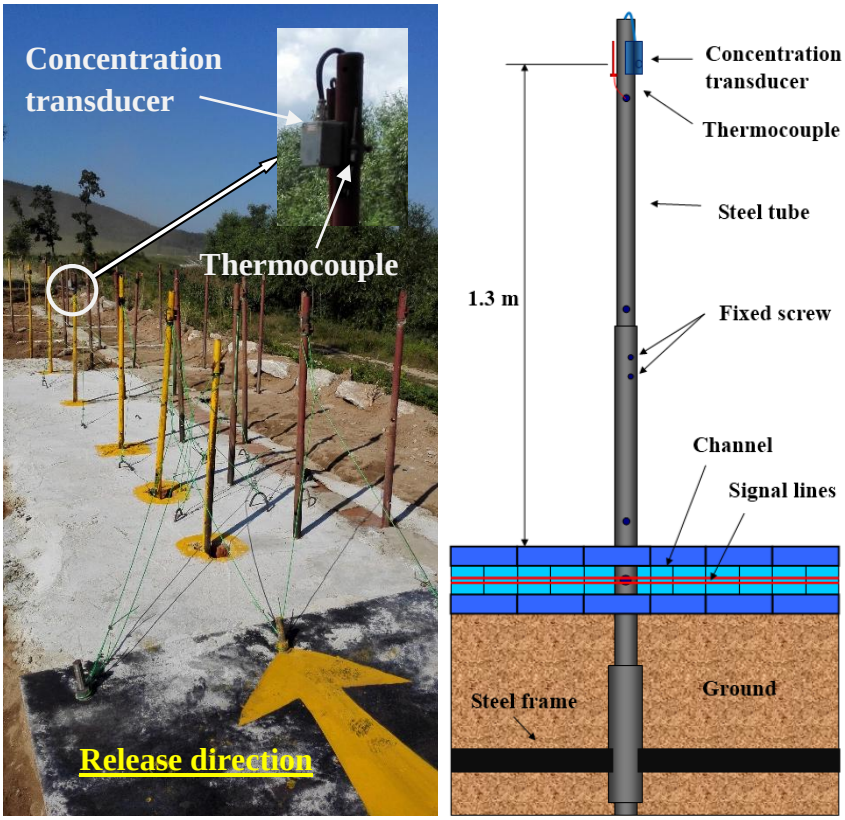

Fig. 3 CO2 concentration sensor and installation.

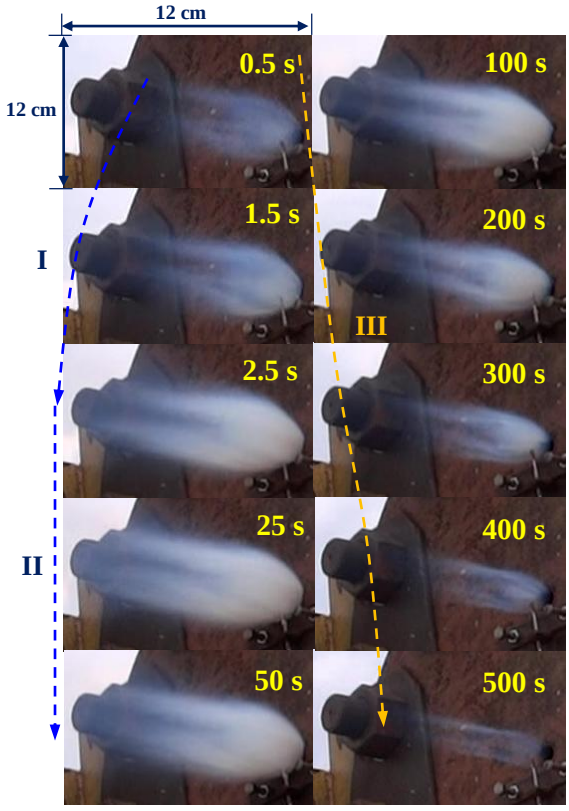

Fig. 4 Visible cloud development of the gaseous CO_2 release experiments with 15 mm orifice.

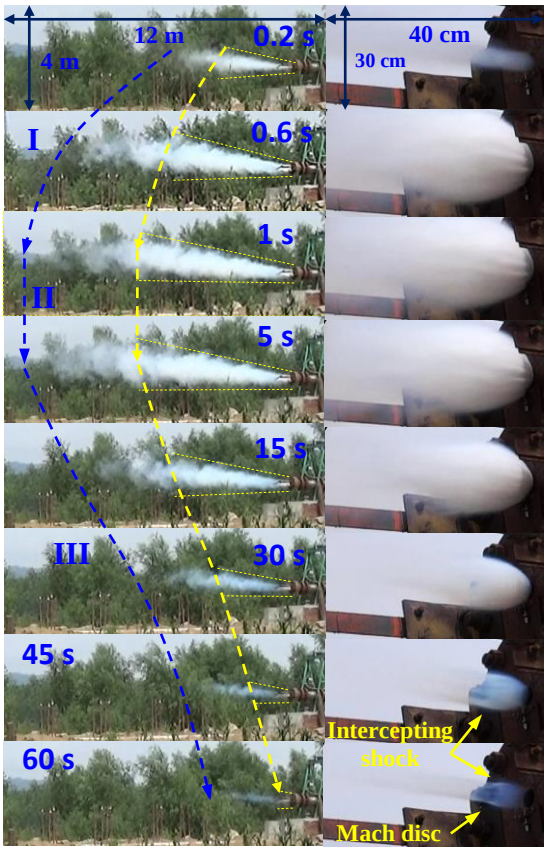

Fig. 5 Visible cloud development of the gaseous CO_2 release experiments with 50 mm orifice.

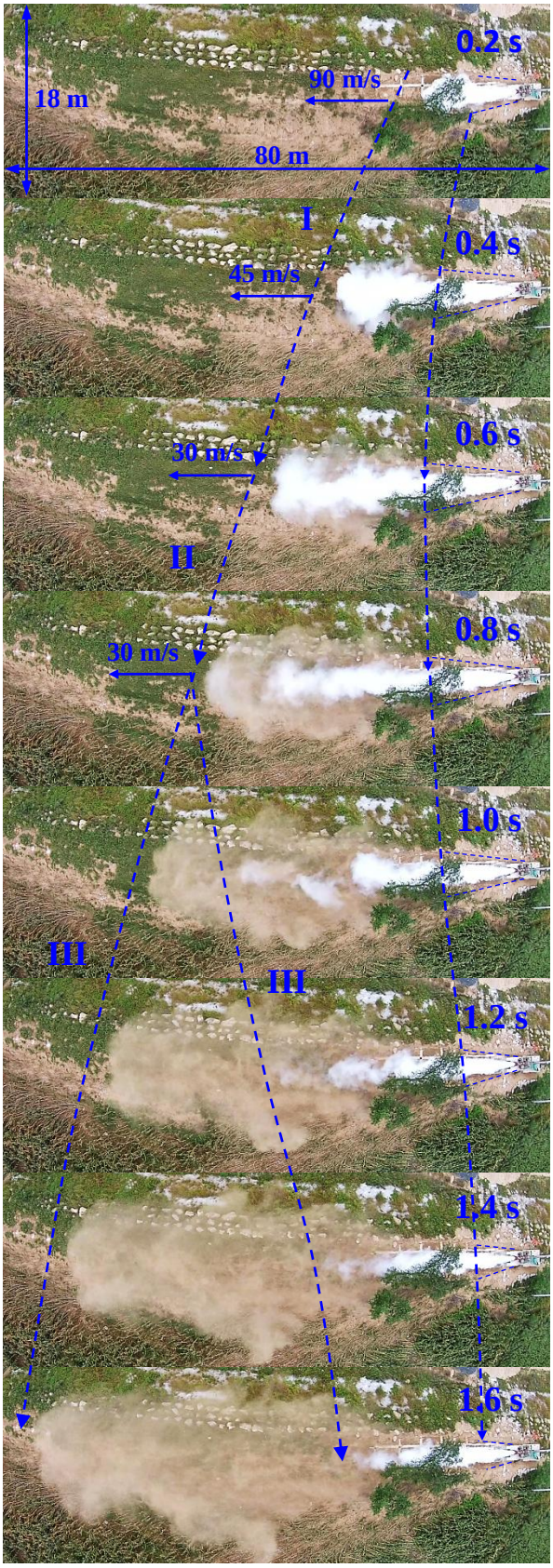

Fig. 6 Visible cloud development of the gaseous CO_2 release experiments with the full bore orifice.

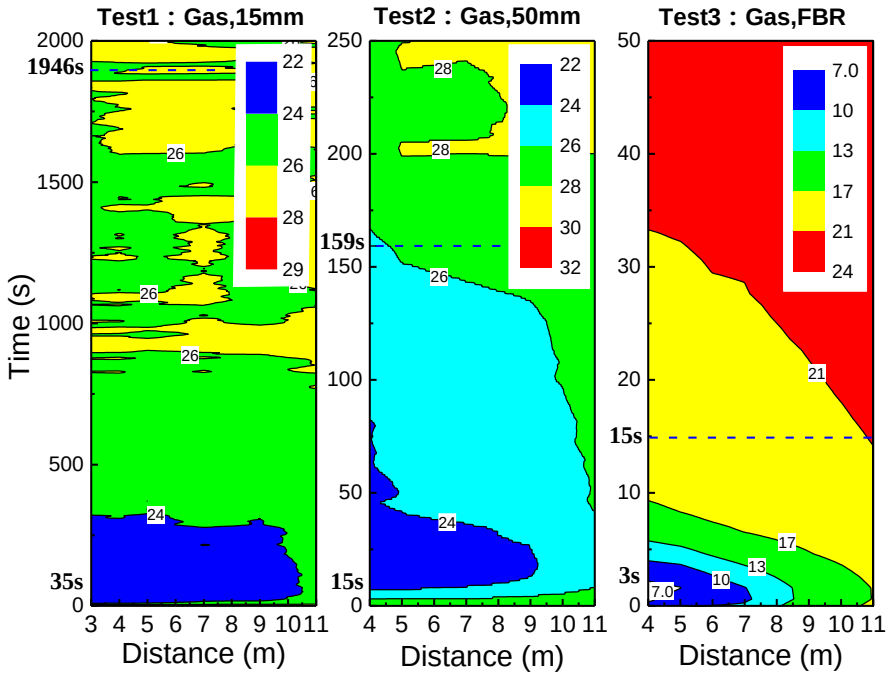

Fig. 7 Temperature evolutions along the centerline of the gaseous CO_2 release experiments with three different orifices (15 mm, 50 mm and FBR).

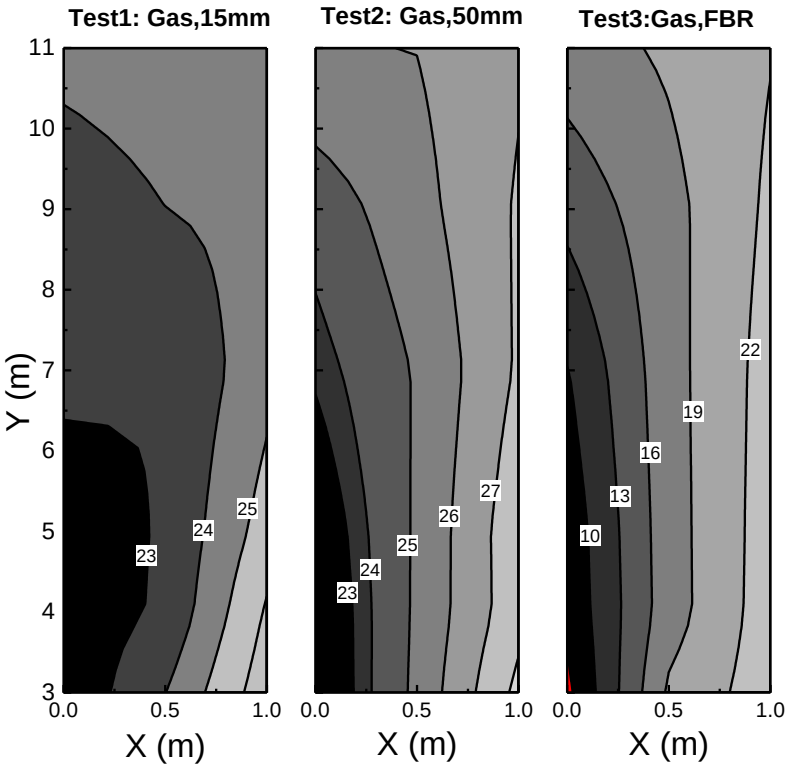

Fig. 8 Temperature distribution area of the gaseous CO_2 release experiments with three different orifices (15 mm, 50 mm and FBR).

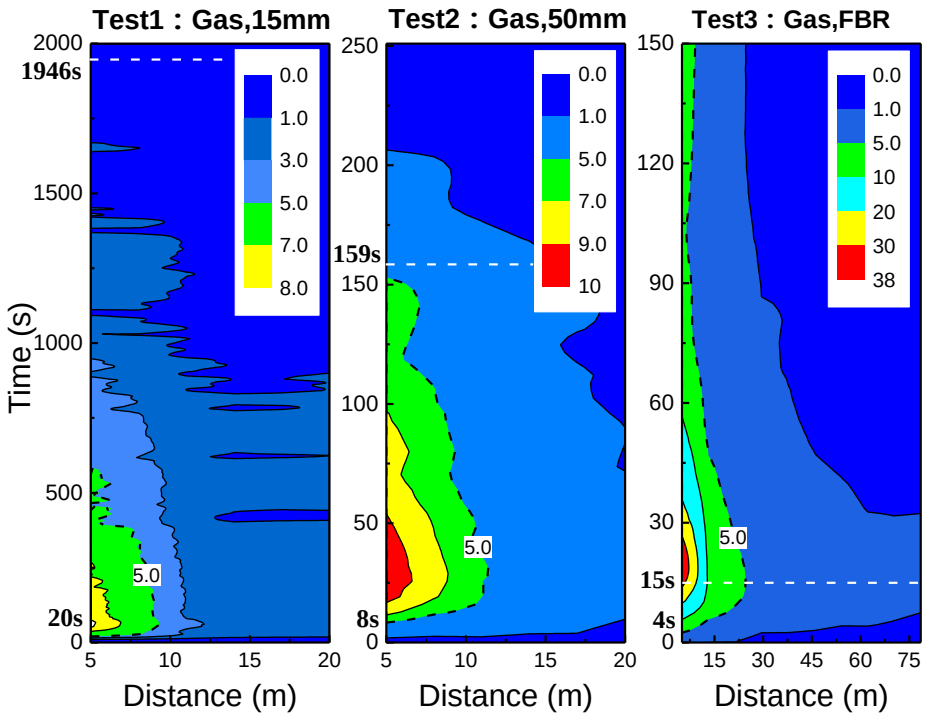

Fig. 9 CO_2 concentration development along the centerline of the gaseous CO_2 release experiments with three different orifices (15 mm, 50 mm and FBR).

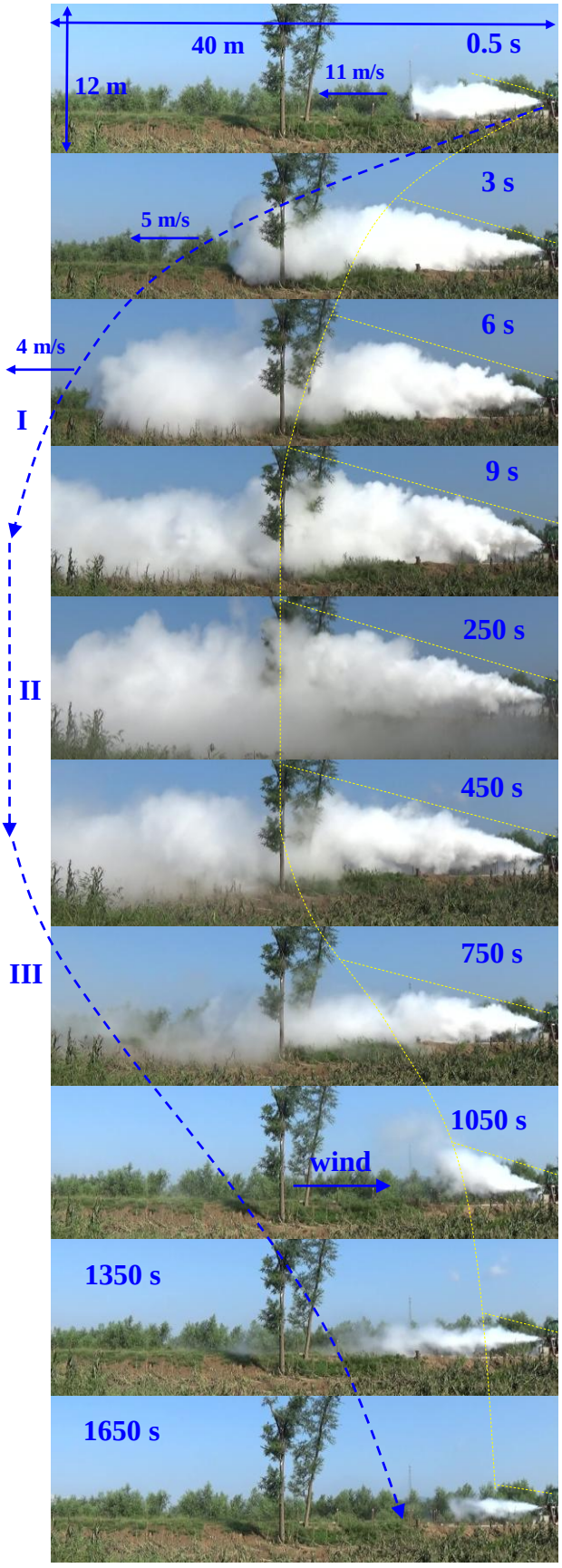

Fig. 10 Visible cloud development of the dense CO_2 release experiments with 15 mm orifice.

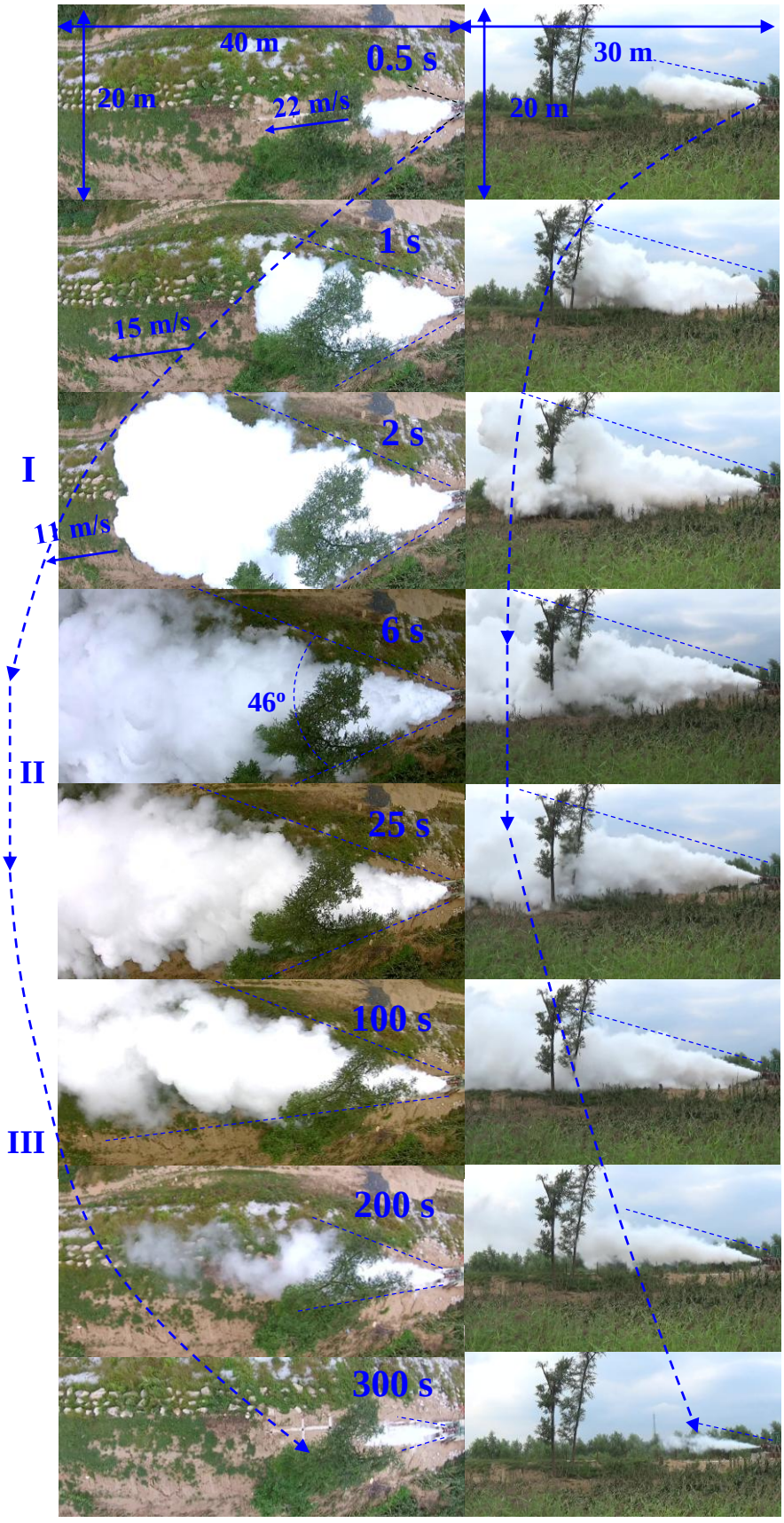

Fig. 11 Visible cloud development of the dense CO_2 release experiments with 50 mm orifice.

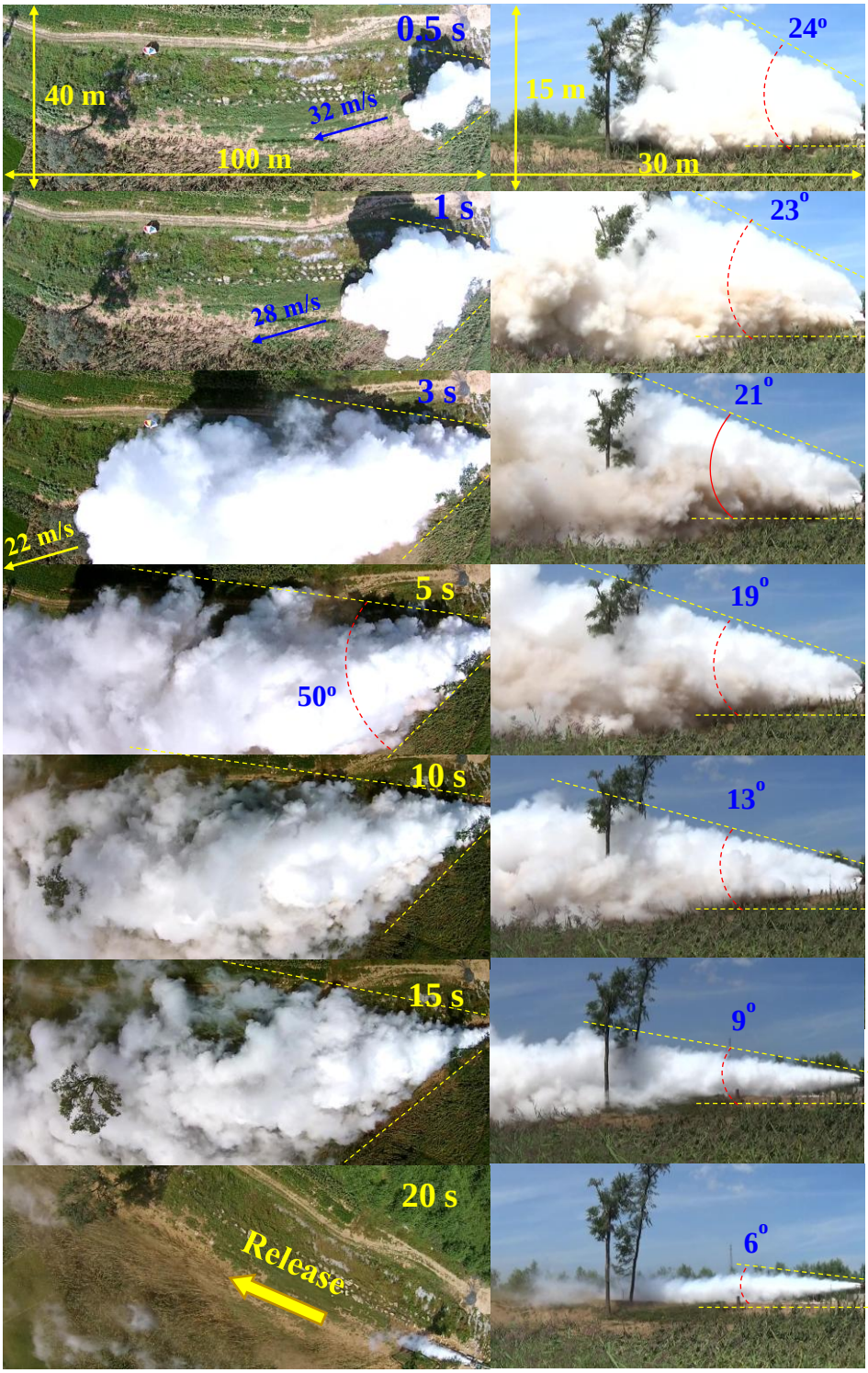

Fig. 12 Visible cloud development of the dense CO_2 release experiments with the full bore orifice.

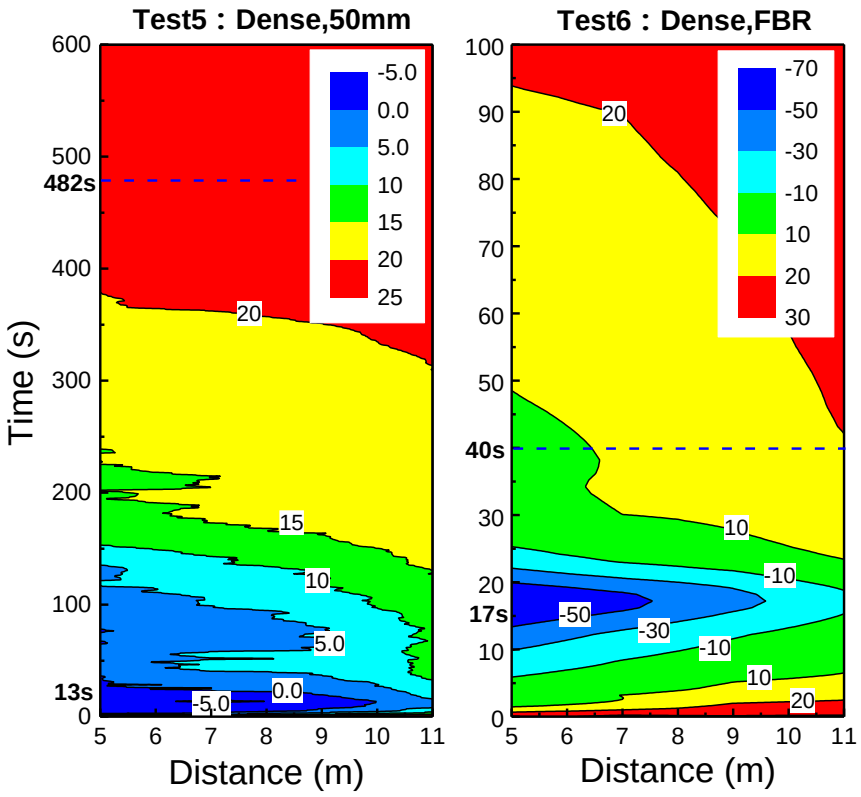

Fig. 13 Temperature evolutions along the centerline of the dense CO_2 release experiments with three different orifices (15 mm, 50 mm and FBR).

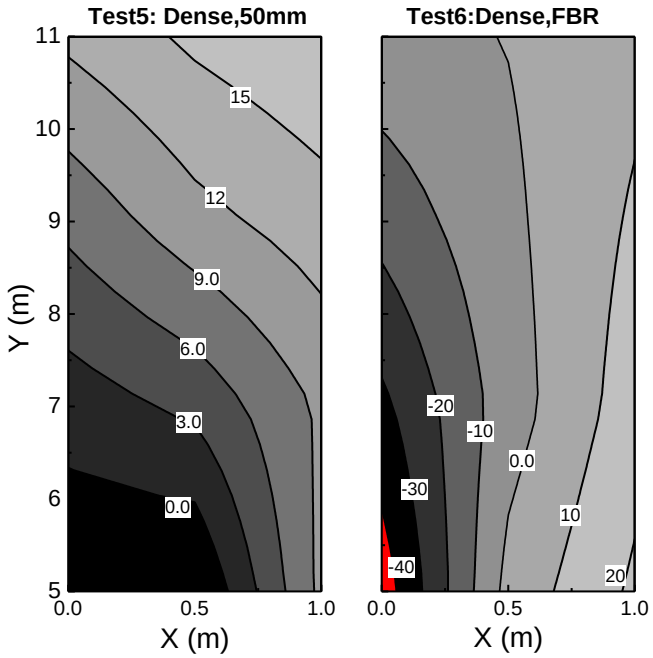

Fig. 14 Temperature distribution area of the dense CO_2 release experiments with three different orifices (15 mm, 50 mm and FBR).

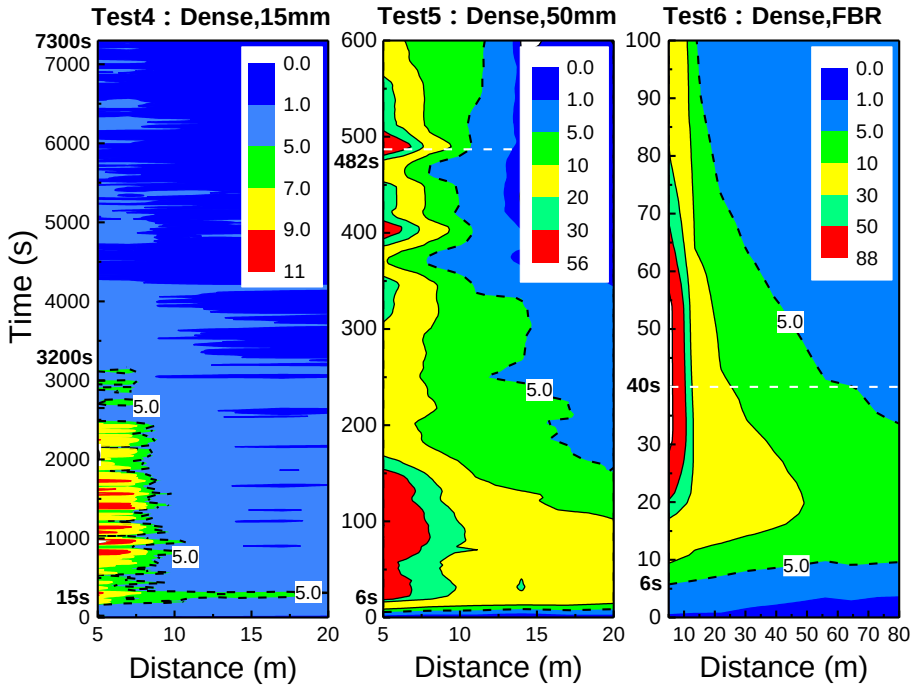

Fig. 15 CO_2 concentration development along the centerline of the dense CO_2 release experiments with three different orifices (15 mm, 50 mm and FBR).